ARTICLE

Journal of Materials Chemistry
www.rsc.org/materials

# Effects of surfactants and synthetic conditions on the sizes and self-assembly of monodisperse iron oxide nanoparticles†

**Xiaowei Teng**[a] **and Hong Yang***[a,b]

[a]*Department of Chemical Engineering, University of Rochester, 253 Gavett Hall, Rochester, New York 14627, USA. E-mail: hongyang@che.rochester.edu*
[b]*Laboratory for Laser Energistics, University of Rochester, Rochester, New York 14627, USA*

***Received 22nd September 2003, Accepted 13th November 2003***
***First published as an Advance Article on the web 5th January 2004***

Monodisperse iron oxide nanoparticles made from the thermal decomposition of iron carbonyl in octyl ether in the presence of oleic and stearic acids have been examined under various reaction conditions. Monodisperse particles with diameters of 3, 5, 10, 16 and 25 nm have been made. Ostwald ripening could be the key reason for making monodisperse nanoparticles with diameters of up to 25 nm, above the largest sizes that have been reported so far for this class of materials. When stearic acid was used as surfactant, the reaction mixtures can reflux at a lower temperature than the reaction using oleic acid, and monodisperse 3 nm $Fe_2O_3$ particles can be made. By controlling the temperatures during the drop casting, different superstructures and superlattices can be created. The nanoparticles and their assembly have been characterized by transmission electron microscopy, electron diffraction, powder X-ray diffraction, and X-ray photoemission spectroscopy.

## Introduction

There has been renewed research interest in high quality monodisperse magnetic nanoparticles in recent years, driven by the new applications of magnetic nanoparticles in advanced magnetic materials,[1–4] ultra high-density magnetic storage media,[1,5,6] biological imaging and therapy.[7–11] Iron oxide and other iron-containing nanoparticles are particularly attractive.[3,5,12] Magnetic nanocomposites of FePt–$Fe_3Pt$ can be made using monodisperse nanoparticles of FePt and $Fe_3O_4$ as precursors.[3] Such magnets can have large energy products, a key indicator of the performance for hard magnetic materials, much higher than single-phased magnets through the so-called exchange coupling mechnism.[3] The use of self-assembly of monodisperse nanoparticles as precursors is also potentially superior over the traditional top-down approaches in terms of processing for large scale production of such advanced magnetic materials.[2] Monodisperse $Fe_2O_3$ nanoparticles have also been used in the synthesis of binary nanocrystalline superlattices, a new class of materials that could have unique magneto-optical properties.[13] In this case, iron oxides have often been chosen as one of the material candidates, and the monodispersity of magnetic nanoparticles is essential.

Monodisperse iron oxide particles of several different shapes at $>100$ nm in length can be synthesized in the aqueous phase through the control of the concentration of inorganic salt precursors and other conditions.[14–16] Nanoparticles of iron and iron oxides with diameters of between 4 and 19 nm have been made, preferably in nonaqueous solvents.[12,17–26] Thermal decomposition of iron carbonyl in organic solvents is an important strategy of making monodisperse iron-containing nanoparticles. The method was first developed in the late 1970s in decalin (*cis*- and *trans*-decahydronaphthalene) and other solvents.[27,28] The decomposition kinetics and its application in making iron-containing nanoparticles have been examined. It was observed that thermal decomposition of $Fe(CO)_5$ first went through an $[Fe(CO)_4]$ intermediate and formed $Fe_m(CO)_n$ nuclei.[27] The further decomposition of $Fe(CO)_5$ on these nuclei followed zero-order kinetics and led to the formation of largely amorphous iron nanoparticles. The nanoparticles formed in this fashion could be readily oxidized.

Recently, this thermal decomposition approach has been successfully used in making monodisperse nanoparticles of FePt alloys, Pt@$Fe_2O_3$, iron and iron oxides with different structures in organic solvents.[5,12,17–19,29,30] The composition, size and size distribution can be finely controlled by varying the reaction mixtures and synthetic conditions. $Fe_2O_3$ nanoparticles with diameters in the range of 4–16 nm can be directly generated with narrow size distribution by introducing an oxidation agent, trimethylamine *N*-oxide, $(CH_3)_3NO$, into the reaction solutions.[18] Several groups have focused the size and composition control of iron oxide nanoparticles derived from this method.

Here we report the effects of surfactants and their concentrations, and the synthetic conditions on the size and size distribution of the monodisperse nanoparticles with diameters between 3 and 25 nm. Although there seems to be no theoretical limit on making large iron oxide nanoparticles, the particles made so far have diameters in the range of 4–19 nm. We present strategies of making $Fe_2O_3$ nanoparticles smaller than 4 nm and larger than 20 nm. Self-assembly of these iron oxide nanoparticles at the enhanced temperatures is also discussed.

## Experimental

### Synthesis of 3 nm particles of iron oxide using stearic acid as surfactant

Iron pentacarbonyl $[Fe(CO)_5$, 30 μL or 0.23 mmol] was added to a mixture of octyl ether (3 mL) and stearic acid (0.1 g or 0.35 mmol) at 100 °C in a 15 mL three-neck round-bottomed flask under an argon flow. A magnetic stirrer was used to provide agitation during the reaction. The mixture was heated to 200 °C at a rate of 2 °C $min^{-1}$. At this temperature, the color of the mixture changed from orange to black, which indicated the formation of nanoparticles. After reaction at this

† Electronic supplementary information (ESI) available: XRD data of iron oxide nanoparticles, Fig. S1 and S2. See http://www.rsc.org/suppdata/jm/b3/b311610g/

DOI: 10.1039/b311610g

 

temperature for 1 h, the mixture was cooled to room temperature. The final product was either stored in the solvent for further characterization or oxidized using $(CH_3)_3NO$ (0.025 g or 0.35 mmol). In the latter case, the mixture was heated to 130 °C under an argon atmosphere and maintained at this temperature for 2 h. The temperature was slowly increased to reflux and the reaction continued for an additional 15 min. The solution was then cooled to room temperature and separated by centrifuge. The resulting solid product can be easily dispersed in hydrocarbon solvents such as hexane, octane and toluene.

### Synthesis of 5 nm particles of iron oxide using oleic acid as surfactant at the reflux temperature

To make 5 nm particles, iron pentacarbonyl [$Fe(CO)_5$, 60 μL or 0.46 mmol] was added to a mixture of octyl ether (3 mL) and oleic acid (440 μL or 1.4 mmol) at 100 °C in a 15 mL three-neck round-bottomed flask under an argon flow. The mixture was then ramped to reflux temperature (290 °C) at 2 °C $min^{-1}$. At this temperature, the mixture still had the orange color that came from the iron carbonyl precursor. After reflux for about 5 to 10 min., the color of the mixture changed abruptly to brown and then to black. The reaction was kept at this temperature for 1 h and cooled to room temperature. Controlled oxidation, if applied, was conducted by adding $(CH_3)_3NO$ (0.05 g or 0.7 mmol) to the reaction mixture. This mixture was then heated to 130 °C under an argon atmosphere and maintained at this temperature for 2 h. The temperature was slowly increased to reflux and the reaction continued for 15 min. After the reaction, the solution was cooled to room temperature and the nanoparticles were separated by centrifuge.

### Synthesis of 10 nm particles of iron oxide using oleic acid as surfactant at the pre-reflux temperatures

In a standard preparation for making 10 nm nanoparticles, octyl ether (3 mL) and oleic acid (440 μL or 1.4 mmol) were added to a 15 mL three-neck round-bottomed flask under an argon flow. After the mixture was heated to 100 °C, iron pentacarbonyl (60 μL or 0.46mmol) was added. The temperature of the mixture was then raised to 275 ± 5 °C at a rate of 2 °C $min^{-1}$, and kept at this temperature for 1 h. The color of the mixture gradually changed from orange to brown, and to black. After the reaction was complete, the reaction flask was cooled to room temperature. Controlled oxidation, if applied, was conducted by using the oxidant $(CH_3)_3NO$ following the procedure described in the previous section.

### Synthesis of >10 nm particles of iron oxide

With the same initial reaction mixture as that for making 10 nm particles but with longer reaction times, particles with diameters larger than 10 nm were obtained. If the mixture was allowed to react at 275 ± 5 °C for 90 min, the diameter of the nanoparticles could reach 16 nm. The diameter of the nanoparticles could reach 25 nm if the heating process lasted for 120 min at 275 ± 5 °C. Particles with average diameters up to 35 nm were synthesized, although the size distribution became broad, and size-selection is required to obtain monodisperse particles.

### Post-synthetic separations

For 3, 5, 10, and 16 nm particles, no size selection was needed. In a typical procedure, a designed amount of the product mixture (200 μL) was transferred into a vial (2 mL) followed by the addition of ethanol to induce the precipitation of the nanoparticles, which were separated from the solvent by centrifugation at 5000 rpm for 5 min. These nanoparticles were recovered by suspension in hexane with a small amount of additional oleic acid (as stabilizer). For 25 nm particles, size selection was required to achieve monodispersity. Typically, ethanol (1.5 mL) was added to the product mixture (200 μL) and nanoparticles precipitated out and were collected after centrifuge. The precipitated particles then then underwent two additional size selection cycles at hexane:ethanol volume ratios of 1:5 and 1:3, respectively. Oleic acid (5 μL/2 mL solvent) was added during the last step of the size selection. The final product was dispersed and stored in hexane. A small amount of oleic acid was required for long-term storage in hexane.

### Self-assembly of nanoparticles

Nanoparticles were spread on the glassy carbon substrates using drop casting. Typically, a drop (*ca.* 0.5 μL) of nanoparticle suspension in hexane (1 mg $mL^{-1}$) was deposited on amorphous, carbon-coated copper mesh at room temperature. Amorphous carbon substrates pre-heated at 50 °C were also used to promote rapid solvent evaporation. In this case, the samples could be dried within a few seconds.

### Characterization

Transmission electron microscope (TEM) images and selected area electron diffraction (SAED) patterns were recorded on a JEOL JEM 2000EX microscope at an accelerating voltage of 200 kV. High resolution TEM images of individual nanoparticles were taken using an ultra-high vacuum scanning transmission electron microscope (UHV-STEM). Powder X-ray diffraction (PXRD) spectra were recorded using a Philips MPD diffractometer with Cu Kα radiation ($\lambda$ = 1.5405 Å). A custom-made silicon wafer was used as substrate for sample measurement. X-Ray photoemission spectroscopy (XPS) was performed using a Surface Science Laboratories SSX-100 instrument equipped with a monochromatic Al anode X-ray gun. Particle size distribution was monitored using Scion Image software (Scion Corporation). For each measurement, about 100–200 particles were used based on the TEM images.

## Results and discussion

Iron oxide particles were prepared *via* the thermal decomposition of $Fe(CO)_5$ in the presence of either oleic acid or stearic acid. Although oleic acid is the more common surfactant used in these systems, both could interact with the particle surfaces as the stabilizers. The decomposition of $Fe(CO)_5$ could be followed experimentally by the change of color of the solutions. The observation of a slow color change from orange to brown, and then the abrupt transition from brown to black afterwards suggested that the reaction could indeed follow zero-order kinetics once the nuclei had formed in the solution.[27] We examined the different parameters which could be used to control the different sizes of the monodisperse nanoparticles of iron oxide. Surfactants and their concentrations, reaction temperatures and durations could all be used in the size and size distribution control of the particles. The oxidation of these iron-containing nanoparticles was also examined with and without the controlled oxidation by $(CH_3)_3NO$.

### Oxidation of iron oxide nanoparticles

In this study we used primarily 10 nm nanoparticles to examine iron oxide in the nanoparticles with and without controlled oxidation by $(CH_3)_3NO$. Fig. 1 shows representative TEM images of oleic acid-stabilized iron oxide nanoparticles before and after oxidation by $(CH_3)_3NO$. The size distribution of these nanoparticles shows the characteristic narrow dispersity for iron-containing nanoparticles made by the thermal decomposition of $Fe(CO)_5$ (Fig. 1a, inset). The size and the dispersity

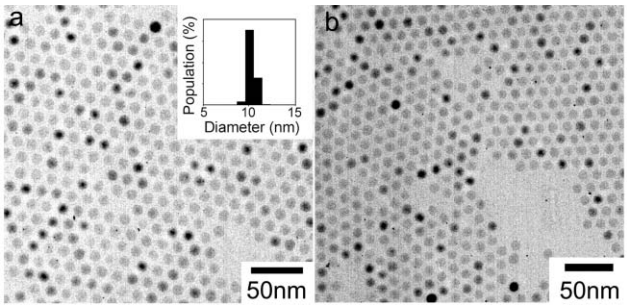


**Fig. 1** TEM images of 10 nm iron oxide nanoparticles (a) without and (b) with oxidation by $(CH_3)_3NO$. Inset: size analysis of obtained nanoparticles.

of the nanoparticles did not seem to be affected by the oxidation process using $(CH_3)_3NO$.

PXRD traces of oleic acid-stabilized iron oxide nanoparticles with or without oxidation by $(CH_3)_3NO$ show no crystalline iron (see Fig. S1, ESI†). The X-ray diffraction patterns from iron oxide can be observed in both samples. The XRD spectra shown in Figure S1a were typically recorded in air within a day of the particles being made. The XRD features of the as-made iron oxide nanoparticles are due to cubic $\gamma$-$Fe_2O_3$ and with some FeO (space group *Fm3m*). It is known that iron can be readily oxidized once it is exposed to air. The oxidation of oleic acid-stabilized iron-containing nanoparticles has been observed for compositions of both iron and its alloys such as FePt.[31] The diffraction peaks at 35.5, 43.1 and 62.5° 2$\theta$ can be indexed as (311), (400), and (440) planes assigned either as $\gamma$-$Fe_2O_3$ (cubic maghemite; space group $P4_232$) or $Fe_3O_4$ (magnetite) because both iron oxides have the inverse spinel structure. Their XRD patterns differ only in the relative intensities of given crystalline planes. The $(CH_3)_3NO$ oxidized and annealed nanoparticles did show relatively narrow diffraction peaks, which indicate they had high crystallinity.

We used XPS to examine the oxidation state of the iron in these nanoparticles, because core electron lines of ferrous and ferric ions can both be detected and are distinguishable from each other in XPS.[19,32,33] Fig. 2 shows the representative XPS spectra for Fe 2p of 10 nm nanoparticles, magnetite ($Fe_3O_4$) and $\gamma$-$Fe_2O_3$ powder samples (from Aldrich). The particular nanoparticles used were washed extensively to remove as much surfactant as possible. The binding energies at 710.9 and 723.5 eV are the characteristic doublet from Fe $2p_{3/2}$ and Fe $2p_{1/2}$ core-level electrons, respectively. These nanoparticles matched not only the peak positions but also the shapes of those for the $\gamma$-$Fe_2O_3$ standard. The shoulder peak between Fe $2p_{3/2}$ (710.9 eV) and Fe $2p_{1/2}$ (723.5 eV) shows primarily in $\gamma$-$Fe_2O_3$, but not in $Fe_3O_4$. No metallic iron signal was detected

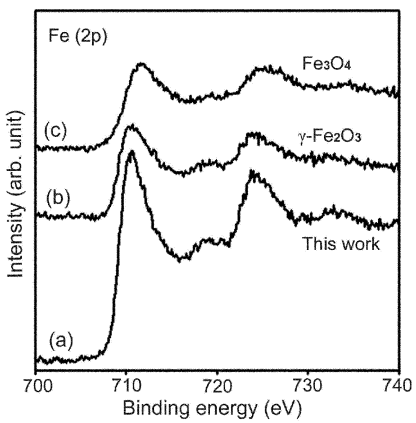


**Fig. 2** XPS spectra for Fe 2p of (a) 10 nm iron oxide nanoparticles without oxidation by $(CH_3)_3NO$, (b) $\gamma$-$Fe_2O_3$, and (c) $Fe_3O_4$ standards.

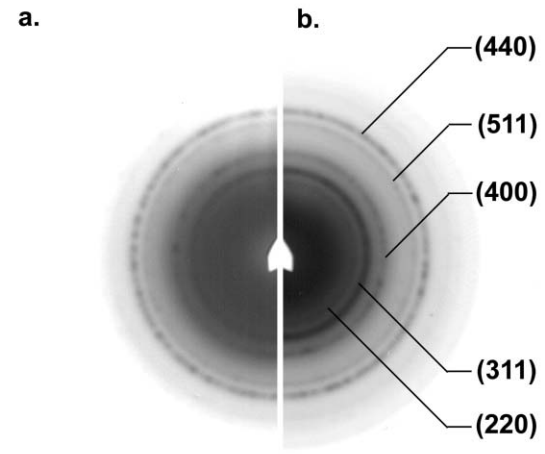


**Fig. 3** SAED micrographs of 10 nm iron oxide nanoparticles (a) without and (b) with oxidation by $(CH_3)_3NO$.

in the XPS spectra. Fig. 3 shows the SAED patterns of these iron oxide nanoparticles. In both cases, diffractions from a series of crystalline planes such as (220), (311), (400), (511) and (440) were observed. The *d*-spacing in these two diffraction patterns was also similar. Fig. 4 summarizes the PXRD, TEM and SAED data for 16 nm iron oxide nanoparticles. No major differences could be observed in the particle size, size distribution, and ED patterns. The PXRD patterns have much narrower peaks for controlled oxidized nanoparticles than those without oxidation by $(CH_3)_3NO$.

PXRD curves for iron oxide-containing monodisperse nanoparticles with diameters between 3 and 25 nm all show $Fe_2O_3$ diffractions without using the oxidation agent, $(CH_3)_3NO$ (see Fig. S2, ESI†). We note that although 3 and 5 nm particles possessed relatively weak and broad diffractions, only those from $\gamma$-$Fe_2O_3$ could be observed. The line broadening could be due to the small particle sizes. In comparison, there were partially oxidized 10 nm iron oxide particles, judging by the fact that the

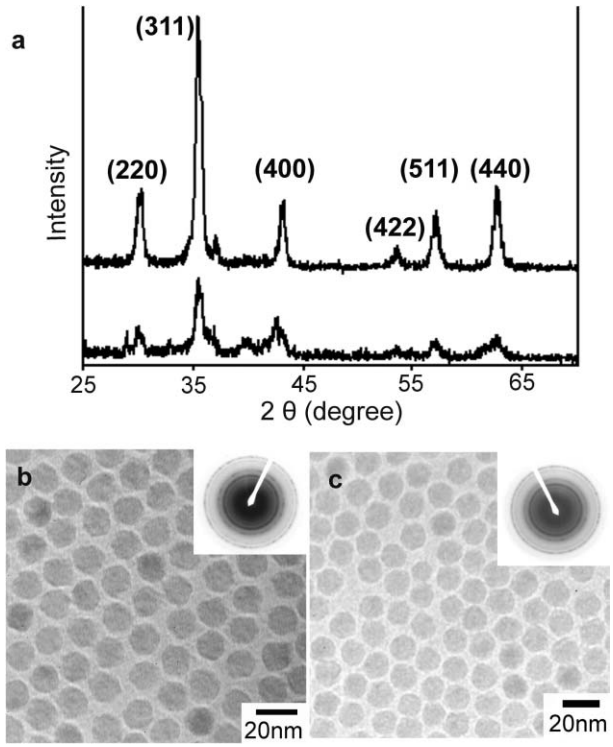


**Fig. 4** (a) XRD spectra and (b, c) TEM micrographs of 16 nm iron oxide particles (b) without and (c) with oxidation by $(CH_3)_3NO$. Insets: SAED patterns of the nanoparticles.

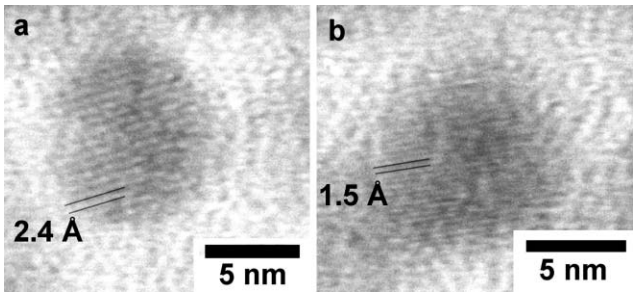


**Fig. 5** HR-TEM images of *ca.* 10 nm nanoparticles showing the (a) (311) and (b) (440) planes of cubic $\gamma$-$Fe_2O_3$.

diffractions at *ca.* 35–36° 2$\theta$ were most likely from $Fe_2O_3$ and FeO (Fig. S2c). It appears that there exists a critical size around 10 nm. Iron oxide particles below this critical size could potentially be fully oxidized without the use of $(CH_3)_3NO$. Fig. 5 shows high resolution TEM images of two *ca.* 10 nm nanoparticles. Both are in single crystalline form showing the (311) (*d*-spacing 2.4 Å) and (440) (*d*-spacing 1.5 Å) fringes of cubic $\gamma$-$Fe_2O_3$. It is possible that the amorphous nature of iron formed through the thermal decomposition of $Fe(CO)_5$ contributes to this relatively deep level oxidation. We note that the large particles (16 and 25 nm) which made for longer reaction times at 275 °C, show relatively strong X-ray diffractions from cubic $\gamma$-$Fe_2O_3$.

### Effect of oleic acid concentrations

We examined the minimum required oleic acid:$Fe(CO)_5$ molar ratio, *n*, for making monodisperse nanoparticles at 275 ± 5 °C,

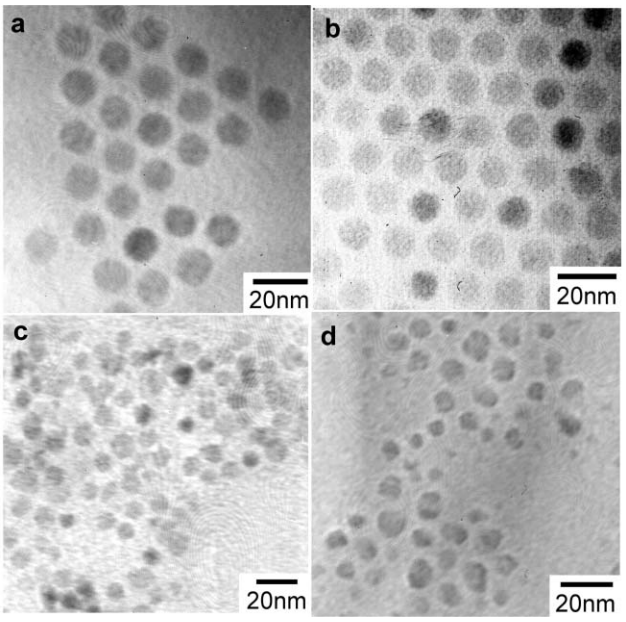


**Fig. 6** Effects of oleic acid:$Fe(CO)_5$ molar ratio, *n*, on the particle sizes and size distributions: *n* = (a) 4, (b) 3, (c) 2 and (d) 1.

which were just below the refluxing temperature. Fig. 6 shows TEM images of such nanoparticles made at oleic acid:$Fe(CO)_5$ molar ratios between 1 and 4 in octyl ether. The reactions were terminated after one hour. We found that when the oleic acid:$Fe(CO)_5$ molar ratio was $<2$, only polydispersed nanoparticles could be observed, which suggests that, at low concentrations, oleic acid is ineffective at stabilizing the iron oxide particles resulting in a broad size distribution. When this ratio was increased to $\geqslant 3$, monodisperse particles were obtained (Fig. 6a and 6b). It appears that the oleic acid:$Fe(CO)_5$ molar ratio of 3 approaches the lower limit for making monodisperse nanoparticles under such synthetic conditions. At the refluxing temperature (*ca.* 290 °C), monodisperse 5 nm nanoparticles could be synthesized using a mixture with same reactant molar ratio.

### Reaction time

One effective strategy for making relatively large nanoparticles is to apply the Ostwald ripening principle in a colloidal reaction system,[34–36] although it does depend highly upon the materials that the nanoparticles are made of. In essence, small nanoparticles dissolve during the prolonged reaction time – the ripening process – and redeposit on the large ones. Fig. 7 shows TEM images of iron oxide nanoparticles obtained with oleic acid:$Fe(CO)_5$ ratio of 3 at 275 °C for a reaction time varied from 60 to 150 min. The diameters of the nanoparticles changed from 10, to 16 and to 25 nm when the reaction time changed from 60 to 90 and to 150 min, respectively. It is noted that unlike the previous report,[18] no further addition of $Fe(CO)_5$ precursor was required for making $Fe_2O_3$ nanoparticles larger than 10 or even 20 nm using this method. Under the reflux conditions, such iron oxide nanoparticles with diameters larger than 11 nm were made by further addition of $Fe(CO)_5$ in the reaction vessel. In that approach, the maximum size that could be obtained was 16 nm in diameter.[18] When the reaction time was longer than 3 h, faceted particles with an average diameter of 35 nm were recovered. The particles, however, became polydisperse in size. The slow consumption of $Fe(CO)_5$ is most likely not the major contributing factor for this time-dependent size growth based on the following observations. The reaction is zero-order in $Fe(CO)_5$ concentration, suggesting that this precursor should be exhausted rapidly after the nucleation step. We observed that the abrupt color change of the reaction mixture happened after reaction took place for about 5–10 min. After reaction for another 15–20 min, we removed a small amount of the samples and examined them using TEM. The TEM images show that these particles are polydisperse, which suggests that Ostwald ripening took place and could be the key reason for the formation of monodisperse nanoparticles.

### Stearic acid as surfactant

Surfactants typically play crucial roles in the particle size and size distribution. We have examined the effect of stearic acid on the particle size and size distribution. Stearic acid was chosen because this surfactant has a similar chain length to oleic acid, except that

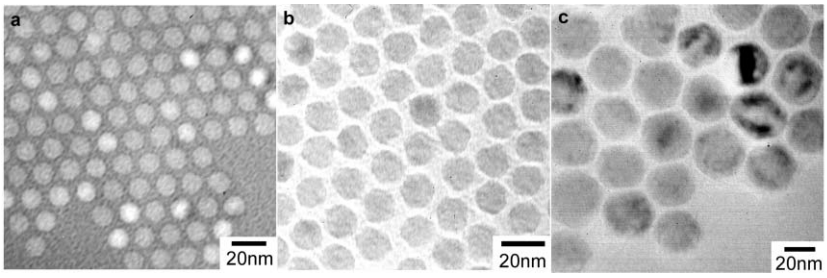


**Fig. 7** TEM images of iron oxide nanoparticles obtained with an oleic acid:$Fe(CO)_5$ molar ratio of 3:1 at 275 °C for a reaction duration of (a) 60 (10 nm), (b) 90 (16 nm), and (c) 150 min (25 nm).

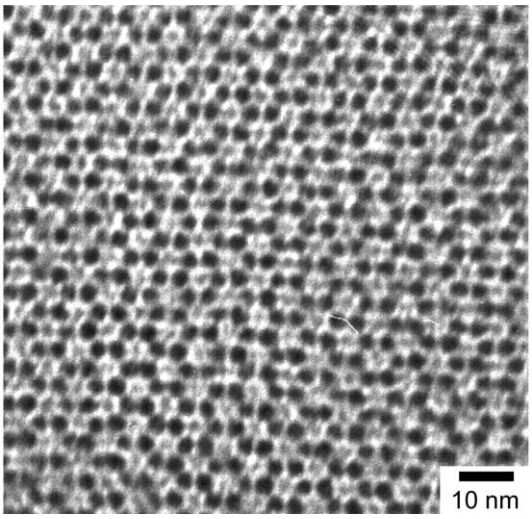


**Fig. 8** Iron oxide nanoparticles synthesized using stearic acid as surfactant. The diameter of the particles is *ca.* 3 nm.

stearic acid does not contain C=C bonds, which can lead to different packing structures on iron oxide surfaces. We were able to obtain highly monodisperse nanoparticles of $\gamma$-$Fe_2O_3$ in octyl ether at a stearic acid:$Fe(CO)_5$ molar ratio of 1.5. Unlike oleic acid, the stearic acid-containing reaction mixtures began to reflux at a much lower temperature of 200 °C. Fig. 8 shows a representative image of such nanoparticles made at this reflux temperature. The average diameter of these particles is 3 nm and such particles diffracted X-rays weakly at 36, 43 and 62° $2\theta$, which correspond to those from the (311), (400), and (440) planes of $\gamma$-$Fe_2O_3$ (see Fig. S2a, ESI†). A previous study on using stearic acid as the capping agent by sonochemical synthesis failed to make monodisperse iron oxide particles, which could be due to the synthetic control in the decomposition of carbonyl compounds.[37] Thermal decomposition seems to be a preferred method in making monodisperse iron oxide nanoparticles. Monodisperse nanoparticles with diameter of 3 nm were also the smallest size that was obtainable using such colloidal systems. The stearic acid:$Fe(CO)_5$ molar ratio of 1.5 was the optimized condition. At a stearic acid:$Fe(CO)_5$ molar ratio of $\geqslant$1.8, the reaction mixture became too viscous to maintain the high stirring rate that is required for homogeneous mixing. As the stearic acid:$Fe(CO)_5$ molar ratio went below about one, nanoparticles with different sizes were observed.

### Self-assembly of iron oxide nanoparticles

One of the characteristics of monodisperse nanoparticles is the ability to form ordered close-packed arrays. In low-dimensional packing structures, the hexagonal array with six-fold symmetry is by far the most common one, although four-fold symmetry is also possible depending upon the particle shapes and surface properties. We were able to create superlattices in both high and low particle densities. The faceted 'single-crystalline' feature of superlattices was observed in both the thin layer and bulk form when the drop casting of particles in hexane was conducted on amorphous carbon substrates at the elevated temperature (50 °C).

Fig. 9 shows the TEM images of the self-assembly of 10 nm oleic acid-stabilized $Fe_2O_3$ nanoparticles (1 mg $mL^{-1}$). Two different packing structures were observed: double- or multiple-layered AB-type stacking, Fig. 9b, and densely close packing, Fig. 9c. Thin films of superlattices in a hexagon shape formed under such condition, Fig. 9d. At a relatively high concentration (3 mg $mL^{-1}$), micron-sized superlattices of 5 nm nanoparticles could be observed in a relatively large populations, Fig. 10a. Under these conditions, the monodisperse nanoparticles seemingly assembled in preference along certain crystalline

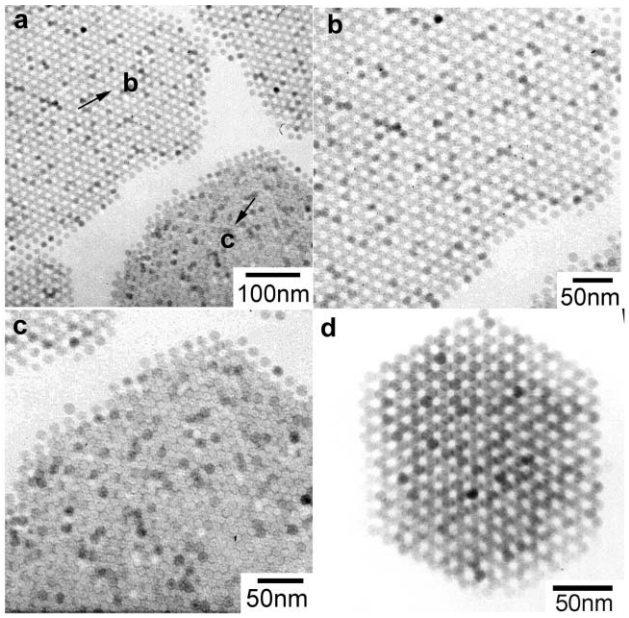


**Fig. 9** Self-assembly of 10 nm iron oxide nanoparticles showing the (a, b) high void:particle and (a, c) low void:particle ratios and (d) a superlattice thin film of hexagonal shape.

directions and led to the formation of hexagonal, Fig 10b, and truncated triangle morphologies, Fig. 10c. Highly ordered arrays of nanoparticles resembling those of the (111) crystalline plane could be found upon close examination of the edges of the hexagon superlattice, Fig. 10d. These micron-sized superlattices were made under rapid nucleation and growth conditions that have been considered as favoring the assembly in a glassy state for surfactant-stabilized quantum dots.[35] For micron-sized superlattices, rapid drying appears to be sufficient and effective.

## Conclusions

Thermal decomposition of $Fe(CO)_5$ in octyl ether in the presence of oleic acid and stearic acid can be an effective

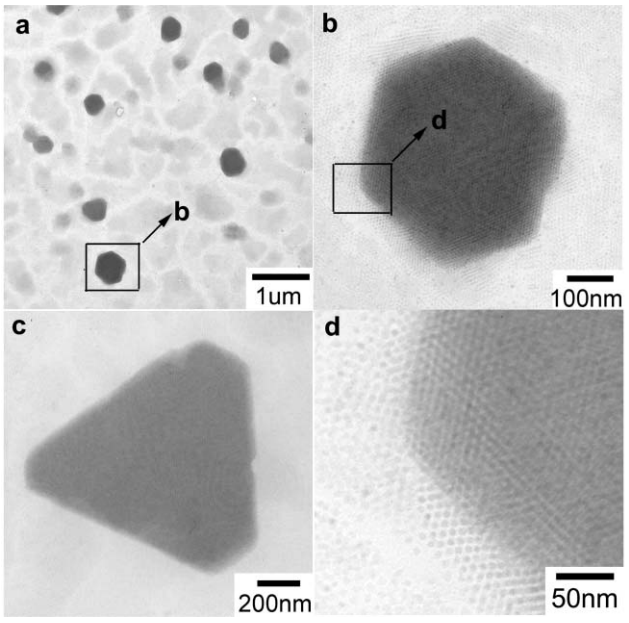


**Fig. 10** TEM images of the self-assembly of 5 nm iron oxide particles generated through rapid solvent evaporation showing (a) a large population of micron-sized superlattices, (b) hexagonal and (c) truncated triangle morphologies, and (d) the edge of the hexagon.

method for making monodisperse iron oxide nanoparticles. Our experiments indicate that the oxidation depth of the as-synthesized iron oxide nanoparticles could reach as far as 4–5 nm without the use of oxidant $(CH_3)_3NO$. Ostwald ripening can be applied in this synthetic system to obtain monodisperse nanoparticles of iron oxide with diameters up to 25 nm. By using stearic acid instead of oleic acid as the surfactant, 3 nm $Fe_2O_3$ particles could be synthesized. The presented approaches can be used to make monodisperse iron oxide nanoparticles beyond the previously reported size range of 4–19 nm.[18,29] Superlattices in both thin film and bulk forms can be obtained under rapid solvent evaporation conditions. The self-assembly of nanoparticles along preferred crystalline directions leads to the formation of hexagonal and truncated triangle shaped superlattices.

## Acknowledgements

This work is supported in part by the University of Rochester and by the U. S. Department of Energy (DE-FC03-92SF19460). We are grateful to LLE for a Horton Fellowship (X. T.). We thank Dr Malcolm Thomas at the Cornell Center for Materials Research (UHV-STEM), Mr Brian McIntyre (TEM) and Dr Yongli Gao (XPS) for technical assistance. The support of the DOE does not constitute an endorsement by the DOE of the views expressed in this article.

## References

1 R. Skomski, *J. Phys.: Condens. Matter*, 2003, R841–R896.
2 D. J. Sellmyer, *Nature*, 2002, **420**, 374–375.
3 H. Zeng, J. Li, J. P. Liu, Z. L. Wang and S. H. Sun, *Nature*, 2002, **420**, 395–398.
4 X. Teng and H. Yang, *J. Am. Chem. Soc.*, 2003, **125**, 14 559–14 563.
5 S. H. Sun, C. B. Murray, D. Weller, L. Folks and A. Moser, *Science*, 2000, **287**, 1989–1992.
6 D. Weller and M. F. Doerner, *Annu. Rev. Mater. Sci.*, 2000, **30**, 611–644.
7 U. Hafeli, W. Schutt, J. Teller and M. Zborowski, *Scientific and Clinical Applications of Magnetic Carriers*, Plenum Press, New York, 1997.
8 I. Safarik and M. Safarikova, *Monatsh. Chem.*, 2002, **133**, 737–759.
9 J. M. Perez, T. O'Loughin, F. J. Simeone, R. Weissleder and L. Josephson, *J. Am. Chem. Soc.*, 2002, **124**, 2856–2857.
10 D. Pouliquen and C. Chouly, in *Magnetic Microcarriers for Medical Applications*, ed. R. Arshady, Citus Books, London, 1999, ch. 12, pp. 343–382.
11 M. Zhao, L. Josephson, Y. Tang and R. Weissleder, *Angew. Chem., Int. Ed.*, 2003, **42**, 1375–1378.
12 T. Hyeon, *Chem. Commun.*, 2003, 927–934.
13 F. X. Redl, K.-S. Cho, C. B. Murray and S. O'Brien, *Nature*, 2003, **423**, 968–971.
14 E. Matijevic, *MRS Bull.*, 1989, **14**, 18–46.
15 M. Ozaki, *MRS Bull.*, 1989, **14**, 35–40.
16 M. Ozaki and E. Matijevic, *J. Colloid Interface Sci.*, 1985, **107**, 199–203.
17 S. H. Sun and H. Zeng, *J. Am. Chem. Soc.*, 2002, **124**, 8204–8205.
18 T. Hyeon, S. S. Lee, J. Park, Y. Chung and H. Bin Na, *J. Am. Chem. Soc.*, 2001, **123**, 12 798–12 801.
19 Q. Guo, X. Teng, S. Rahman and H. Yang, *J. Am. Chem. Soc.*, 2003, **125**, 630–631.
20 T. Fried, G. Shemer and G. Markovich, *Adv. Mater.*, 2001, **13**, 1158–1161.
21 J. Lu, J. D. Fan, R. S. Xu, S. J. Roy, N. Ali and Y. Gao, *J. Colloid Interface Sci.*, 2003, **258**, 427–431.
22 S. Thimmaiah, M. Rajamathi, N. Singh, P. Bera, F. Meldrum, N. Chandrasekhar and R. Seshadri, *J. Mater. Chem.*, 2001, **11**, 3215–3221.
23 M. Rajamathi, M. Ghosh and R. Seshadri, *Chem. Commun.*, 2002, 1152–1153.
24 J. Rockenberger, E. C. Scher and A. P. Alivisatos, *J. Am. Chem. Soc.*, 1999, **121**, 11 595–11 596.
25 Y. S. Kang, S. Risbud, J. Rabolt and P. Stroeve, *Langmuir*, 1996, **12**, 4345–4349.
26 M. D. Bentzon, J. Vanwonterghem, S. Morup and A. Tholen, *Philos. Mag. B-Phys. Condens. Matter Stat. Mech. Electron. Opt. Magn. Prop.*, 1989, **60**, 169–178.
27 T. W. Smith and D. Wychick, *J. Phys. Chem.*, 1980, **84**, 1621–1629.
28 C. H. Griffiths, M. P. Ohoro and T. W. Smith, *J. Appl. Phys.*, 1979, **50**, 7108–7115.
29 D. Farrell, S. A. Majetich and J. P. Wilcoxon, *J. Phys. Chem. B*, 2003, **107**, 11 022–11 030.
30 X. W. Teng, D. Black, N. J. Watkins, Y. L. Gao and H. Yang, *Nano Lett.*, 2003, **3**, 261–264.
31 S. H. Sun, S. Anders, H. F. Hamann, J. U. Thiele, J. E. E. Baglin, T. Thomson, E. E. Fullerton, C. B. Murray and B. D. Terris, *J. Am. Chem. Soc.*, 2002, **124**, 2884–2885.
32 R. M. Cornell and U. Schwertmann, *The Iron Oxides: Structure, Properties, Reactions, Occurrence and Uses*, VCH, Weinheim, 1996.
33 T. Fujii, F. M. F. de Groot, G. A. Sawatzky, F. C. Voogt, T. Hibma and K. Okada, *Phys. Rev. B*, 1999, **59**, 3195–3202.
34 A. L. Rogach, D. V. Talapin, E. V. Shevchenko, A. Kornowski, M. Haase and H. Weller, *Adv. Funct. Mater.*, 2002, **12**, 653–664.
35 C. B. Murray, C. R. Kagan and M. G. Bawendi, *Annu. Rev. Mater. Sci.*, 2000, **30**, 545–610.
36 Y. Sun, B. Mayers, T. Herricks and Y. Xia, *Nano Lett.*, 2003, **3**, 955–960.
37 K. S. Suslick, M. M. Fang and T. Hyeon, *J. Am. Chem. Soc.*, 1996, **118**, 11 960–11 961.